Fabricating Gold Nanocomplexes of Controllable Size Using Electrochemical Oxidation−Reduction Cycling of Gold Substrates in Aqueous Solution

Yu-Chuan Liu,* Hsueh-Hsin Peng

Department of Chemical Engineering, Vanung University, 1, Van Nung Road, Shuei-Wei Li, Chung-Li City, Taiwan, Republic of China

Received: February 5, 2004; In Final Form: August 9, 2004

We report the first electrochemical method to prepare Au-containing nanocomplexes with controllable particle size via roughening gold substrates with oxidation−reduction cycles (ORC) of various scans in 0.1 N KCl aqueous solutions without the addition of any stabilizer. The prepared nanocomplex size increases from 2 to 50 nm with the increase of the ORC scan from 25 to 400 cycles. Furthermore, polypyrrole (PPy)-coated gold nanocomposites can be synthesized by the formation of self-assembled layers and further autopolymerization of pyrrole monomers on these nanocomplexes, caused by their activities.

Introduction

Nanoparticles of noble metals are of great interest today because of their interesting optical,[1] electrochemical,[2] photoelectrochemical,[3] and electronic[4] properties, which can result in the appearance of a new function different from the corresponding bulk material.[5] Recently, various methods have been developed to fabricate nanoparticles. They include chemical reduction,[6] sonochemical reduction,[7] electron beam lithography,[8] laser ablation,[9] radiolytic reduction,[10] metal evaporation,[11] and Ar^+ ion sputtering.[4] Mizukoshi et al.[7] reported colloidal dispersions of bimetallic nanoparticles composed of gold and palladium prepared by a sonochemical method, in which Au(III) and Pd(II) ions in an aqueous solution were reduced by ultrasonic irradiation in the presence of sodium dodecyl sulfate. It is well-known that the prepared nanoparticles demonstrate special size- and shape-dependent properties.[12,13] Therefore, preparation of size-selected metal nanoparticles is one of the important subjects in chemistry and physics of nanoscale materials.[14−18] Mafune et al.[14] reported the formation of gold nanoparticles by laser ablation in an aqueous solution containing surfactants. It was found that the size of the nanoparticles decreases with an increase in the surfactant concentration. Haynes and Van Duyne[15] developed a technique of nanosphere lithography capable of producing size-tunable noble metal nanoparticles in the 20−1000 nm range. This technology, which is based on solid substrates, can be used to fabricate an unexpectedly large variety of nanoparticle structures and well-ordered 2D nanoparticle arrays. They also found that the nanoparticle size and shape have significant effects on the localized surface plasmon resonance spectrum of Ag nanoparticles. Kobayashi Mafune et al.[16] reported sol−gel processing of silica-coated gold nanoparticles which shows the potential for the preparation of gels with different particle sizes and shapes. However, metal nanoparticles are stable only as suspensions in solutions for a short lifetime and tend to irreversibly aggregate over time if no stabilizer is employed. This nature depresses their nanoscale properties and limits their applications. Some stabilizers, such as sodium dodecyl sulfate[7] and sugar-persubstituted poly(amidoamine) dendrimers,[19] were used, and some stabilization technologies of thiol-ligand coatings[20,21] were thus developed to prevent the prepared nanoparticles from aggregating. Moreover, as shown in the literature,[22] diblock copolymers were used to provide small compartments, inside which particles of a finite size can be formed and stabilized. In engineering applications, conducting polymer-supported catalysts are attractive materials for fuel cell design.[23] Also, directly attached polypyrrole (PPy) films provide fast thermal energy transfer pathways for the core gold nanoparticles.[24]

In our previous study, we found that PPy with enhanced conductivity can be prepared by electropolymerization on an electrochemically roughened Au substrate.[25] In this study, a new and easy electrochemical method is developed to prepare Au−Cl nanocomplexes, which means Au−Cl complexes with nanosized, controllable particle sizes achieved via roughening gold substrates with different oxidation−reduction cycles (ORC) in 0.1 N KCl aqueous solutions without addition of any stabilizer. Meanwhile, these nanocomplexes, which are distinguishable from the elemental metal nanoparticles generally reported in the literature, can not only adsorb adsorbates to form self-assembled monolayers (SAMs) but also oxidize them, because of their electrochemical activities.

Experimental Section

Chemical Reagents. Pyrrole (Py) was triply distilled until a colorless liquid was obtained and was then stored under nitrogen before use. KCl was used as received without further purification. The reagents (p.a. grade) were purchased from Acros Organics. All of the solutions were prepared using deionized water of 18 MΩ cm resistivity.

Preparation of Au-Containing Nanocomplexes and Au/PPy Nanocomposites in Solution. All of the electrochemical experiments were performed in a three-compartment cell at room temperature, 22 °C, and were controlled by a potentiostat (model PGSTAT30, Eco Chemie). A sheet of Au with thickness of 0.5 mm, a sheet of platinum, and a KCl-saturated silver−silver chloride (Ag/AgCl) rod were employed as the working, counter, and reference electrodes, respectively. Before the ORC treatment, the Au electrode was mechanically polished (model Minimet 1000, Buehler) successively with 1 and 0.05 μm of

* Corresponding author. Phone: 886-3-4515811 ext. 540. Fax: 886-2-86638557. E-mail: liuyc@msa.vnu.edu.tw.

10.1021/jp0401067 CCC: $27.50
Published on Web 09/29/2004

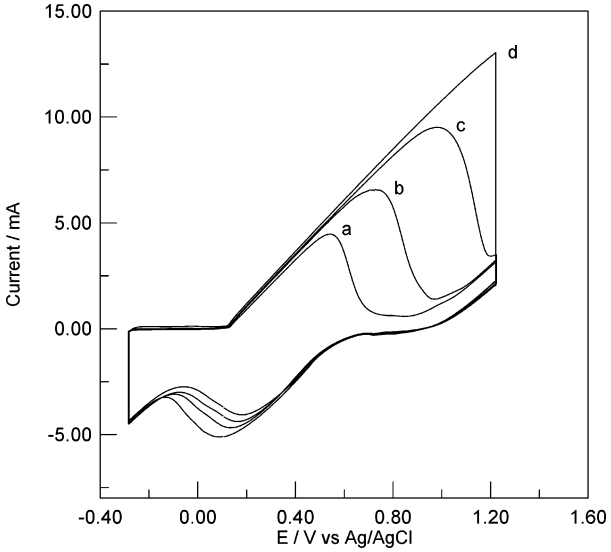

Figure 1. Cyclovoltammograms of different scans of the redox processes occurring on Au substrate in 0.1 N KCl at 500 mV/s; curves a−d represent 25, 50, 100, and 400 scans, respectively.

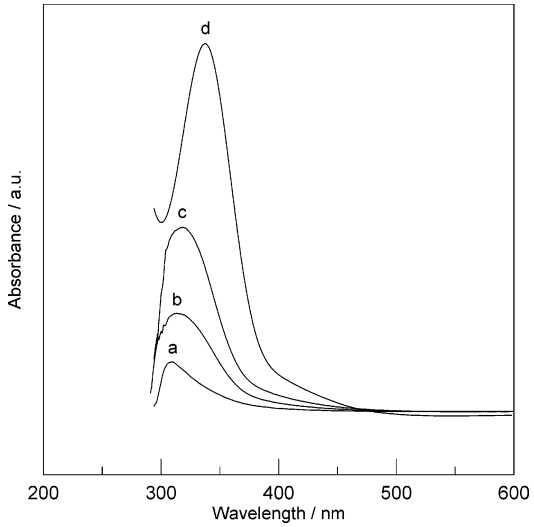

Figure 2. UV−vis spectra of Au-containing nanocomplexes in solutions after roughening Au substrate with different scans; curves a−d represent 25, 50, 100, and 400 scans, respectively.

alumina slurry to a mirror finish. Then, the electrode was cycled in a deoxygenated aqueous solution of pH 5.4 containing 0.1 N KCl from −0.28 to +1.22 V vs Ag/AgCl at 500 mV/s with different scans. The durations at the cathodic and anodic vertexes were 10 and 5 s, respectively. This ORC procedure corresponds to the maximum surface-enhanced Raman scattering of PPy deposited on the roughened Au.[26] The pH of the solutions after 25, 50, 100, and 400 scans were 6.7, 6.7, 6.7, and 6.9, respectively. Then, the Au−Cl nanocomplexes were formed by the anodic oxidation of the Au-substrate electrode in the presence of Cl^- ions in aqueous solution. Subsequently, different amounts of 0.05, 0.1, 0.2, and 0.5 mmol/L pyrrole monomer were individually added to this Au-containing aqueous solution, and the mixture was stirred for 10 min at room temperature in a dark atmosphere to prepare Au/polypyrrole (PPy) nanocomposites.

Characteristics of Au-Containing Nanocomplexes and Au/PPy Nanocomposites in Solution. A single drop of the sample-containing solution was placed on a 300 mesh Cu/carbon film transmission electron microscopy (TEM) sample grid and dried in a vacuum oven. Then, the sample was examined using a JEOL JEM-4000 EX electron microscope with an acceleration voltage of 400 kV. Before recording the XPS spectra, a few drops of sample were evaporated on an amorphized graphite substrate. For the XPS measurements, a Physical Electronics PHI 1600 spectrometer with monochromatized Mg Kα radiation, 15 kV and 250 W, and an energy resolution of 0.1−0.8% $\Delta E/E$ was used. To compensate for surface charging effects, all XPS spectra are referred to the C 1s neutral carbon peak at 284.6 eV. UV−vis absorption spectroscopic measurements were carried out on a Perkin-Elmer Lambda 25 spectrophotometer in 1-cm quartz curvettes.

Results and Discussion

Figure 1 shows the redox process occurring on the gold substrate and the formation of Au−Cl nanocomplexes by the anodic oxidation of the Au-substrate electrode in the presence of Cl^- ions with consecutive scans. The detailed roughening mechanism has been shown elsewhere.[27] The anodic peak becomes larger, and the peak potential anodically increases with an increased number of scans. Also, the anodic current increases with successive scans. The onset of gold dissolution, occurring at approximately 0.9 V vs Ag/AgCl, forms predominantly $AuCl_4^-$ deposited on Au substrate.[28] The oxygen evolution occurs significantly in competition with gold dissolution at a potential more positive than 1.0 V vs Ag/AgCl. With an increasing number of scans, the pale yellow color of the aqueous solution containing positively charged Au- and negatively charged Cl-containing nanocomplexes with nanostructures, as confirmed from XPS and TEM analyses, becomes significantly enhanced. This indicates that the concentration of Au-containing nanocomplexes, which means Au-containing complexes with nanosized particles, increases with an increased number of scans.

Figure 2 shows the UV−vis spectra of Au-containing nanocomplexes in solution after roughening the Au substrate with different scans. Clearly, the absorbance maximum of Au-containing nanocomplexes appears at approximately 320 nm, which is markedly different from that of zero-valent Au at ca. 520 nm.[12,29] Meanwhile, the absorbance maximum demonstrates a monotonic red shift from 308 to 336 nm, which reflects on the corresponding increase of the average particle diameter of these nanocomplexes[19,29] with an increasing number of scans. It means that the particle size of the prepared Au-containing nanocomplexes can be readily controlled by varying the number of scans. The actual particle size was examined by using TEM.

Figure 3a shows the dispersion and the particle size of Au-containing nanocomplexes in a 0.1 N KCl aqueous solution after roughening the Au substrate by ORC treatment 25 times. The nanocomplexes with a mean diameter of ca. 2 nm demonstrate no aggregation and fairly even dispersion but not a perfect spherical shape. This phenomenon may be ascribed to the fact that they are composed of positively charged Au and negatively charged Cl, which can be confirmed from the UV−vis adsorption spectrum and from the XPS analysis, as shown and discussed before and later, respectively. Figure 3b shows the Moiré patterns of the Au-containing nanocomplexes. It slightly exhibits a one-dimensional fringe lattice due to Moiré interference, showing that these nanocomplexes are crystalline by themselves.[20] The corresponding particle sizes of the prepared nanocomplexes are ca. 2, 8, 20, and 50 nm for roughening the Au substrate by ORC treatment with 25, 50, 100, and 400 scans, respectively, as demonstrated in Table 1. By increasing the ORC scans, more Au-containing nanocomplexes are produced in solution by the anodic oxidation of the Au-substrate electrode

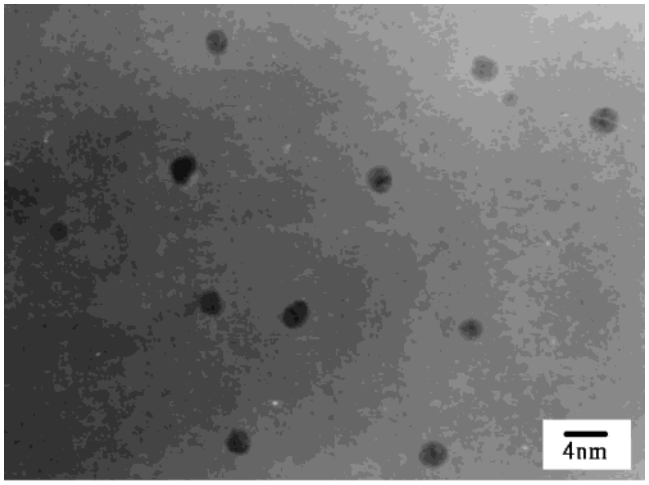

(a)

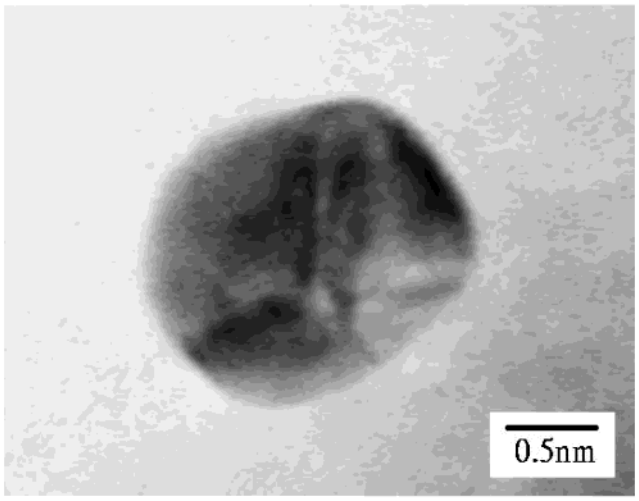

(b)

Figure 3. TEM micrograph of Au-containing nanocomplexes, showing (a) size and dispersion, (b) Moiré fringes.

TABLE 1: Sizing Information on Au-Containing Nanocomplexes in Solutions after Roughening Au Substrate with Different Scans

number of scans	mean diameter (nm)	min (nm)	max (nm)
25	2	1.1	2.8
50	8	4.6	11.3
100	20	13.8	24.6
400	50	38.2	60.2

in the presence of Cl^- ions. This results in more chances for them to aggregate, and thus, larger particle sizes are observed.

Combining the results shown in Figure 2, we can correlate the particle size with the absorption spectra of the solution/colloidal suspension, as shown in Figure 4. The absorption maximum band of the prepared nanocomplexes increases with an increase in size of the corresponding nanocomplex. This phenomenon of a red shift with increased particle size is consistent with results generally reported in the literature.[19,29] This red shift can be ascribed to the interparticle plasmon coupling upon aggregation with an increase in size of the corresponding nanocomplex.

Figure 5 shows the XPS Au $4f_{7/2-5/2}$ core-level spectra of the Au-containing nanocomplexes in solution both after roughening the Au substrate with 100 scans and the Au substrate

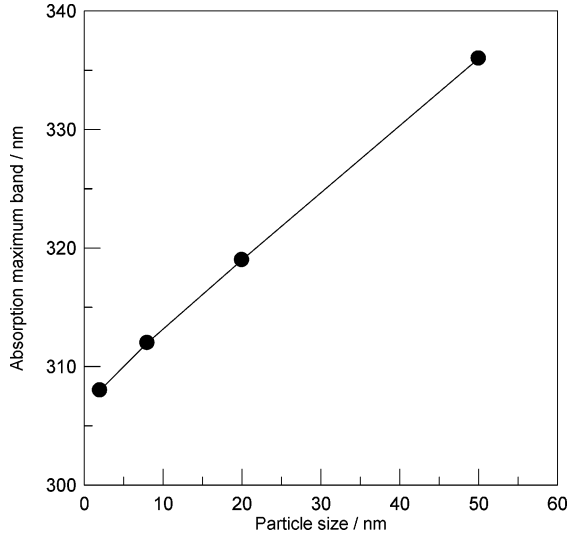

Figure 4. Correlation of absorption maximum band of prepared Au-containing nanocomplexes with their corresponding particle sizes obtained by roughening the Au substrates with different scans in solution.

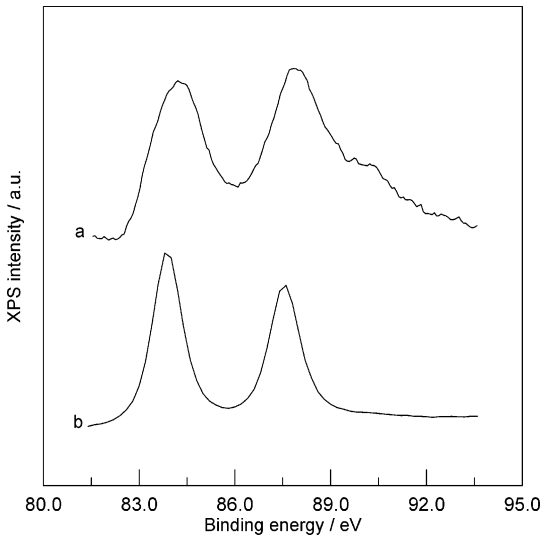

Figure 5. XPS Au $4f_{7/2-5/2}$ core-level spectra of Au-containing nanocomplexes in solution after roughening Au substrate with 100 scans (curve a) and Au substrate before ORC treatment (curve b).

before ORC roughening treatment. As shown in spectrum b, the doublet peaks located at 84 and 87.7 eV can be assigned to Au(0)[30] for the Au substrate before ORC treatment. When comparing spectrum a of the Au-containing nanocomplexes with higher binding energies with spectrum b of the zero-valent Au, we see that the oxidized Au in the Au-containing nanocomplexes can be assigned to monovalent Au(I) and trivalent Au(III) at 85.2 and 86.7 eV, respectively.[31] No further deconvolution was made, and trivalent Au(III), as is usually shown in the Cl- and Au-containing complex,[30,32] was adopted in this study. Also, the XPS Cl 2p core-level spectrum of these nanocomplexes shows the main peak located at ca. 199 eV, which can be assigned to Cl(−1). Because the XPS spectra are similar to those observed on the roughened Au substrates, as has been shown before,[27,33] the Cl- and Au-containing nanocomplexes can be assigned to $AuCl_4^-$. By increasing the number of ORC cycles, we can increase the concentration of the Au-containing nanocomplexes, but the compositions of these nanocomplexes are similar. Because it would be featureless in a TEM image if the solution only contained $AuCl_4^-$ ions, and the UV−vis absorption

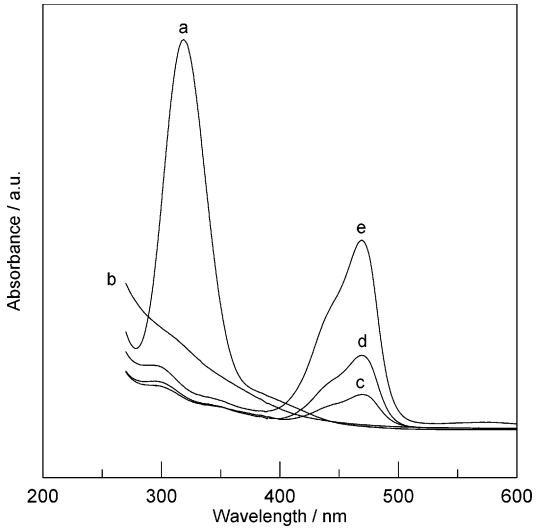

Figure 6. UV−vis spectra of Au-containing nanocomplexes in solution after roughening Au substrate with 100 scans (a), and after subsequently dropping different amounts of pyrrole monomer for 10 min: Spectra b−e represent 0.05, 0.1, 0.2, and 0.5 mmol/L pyrrole monomer added, respectively.

spectrum reveals that the particles on the surface of the Au-containing nanocomplexes would not be zero-valent Au, because its localized surface plasmon resonance is not observed, the structure of the Au-containing nanocomplexes prepared in this study can be proposed as small clusters of a zero-valent Au core with a $AuCl_4^-$ shell. Because the measuring depth of XPS analysis is much deeper than that of UV−vis absorption analysis, we can also see the slight signal of the core of zero-valent Au in the XPS spectrum, but the surface plasmon of zero-valent Au is not observed in the UV−vis absorption spectrum. Combined with the observation from the Moiré patterns in TEM analysis, we see that the prepared Au-containing nanocomplexes are crystalline.

Figure 6a shows the UV−vis spectrum of the $AuCl_4^-$ nanocomplex solution after roughening the Au substrate with 100 scans. After subsequent addition of 0.05 mmol/L pyrrole monomers, the absorbance band of $AuCl_4^-$ nanocomplexes at 319 nm disappears, as shown in Figure 6b. It can be ascribed to the reduction of $AuCl_4^-$ accompanied with the oxidation of pyrrole monomers. In this case, pyrrole monomers are oxidized to polypyrrole in very low concentration. Because of this, the polymer cannot be detected in the UV−vis analysis. On the other hand, $AuCl_4^-$ nanocomplexes are decomposed to smaller particles, and part of them are correspondingly reduced. The produced Au particles are too small to exhibit any surface plasmon absorption,[12] as shown in Figure 6b. Further XPS experiments confirm the presence of polypyrrrole and positively charged Au in the solution after the measurement of spectrum 6b. With increasing amounts of pyrrole monomer, a new band of the $\pi-\pi^*$ transition of PPy[34] in the region of 400−500 nm with an absorbance maximum at ca. 469 nm instead arises with increasing intensity, as shown in spectra c, d, and e of Figure 6. The polymerization of pyrrole monomer is an oxidation reaction. The positively charged Au in the nanocomplexes can oxidize the pyrrole monomer to form polypyrrole-coated Au nanocomposites. In this formation, the positively charged Au is reduced to its elemental state. Figure 7 demonstrates distinguishable dark cores surrounded by grayish shells of PPy. The size distributions are relatively wide and the shapes are somewhat elongated because of the oxidation polymerization of pyrrole occurring on multiple $AuCl_4^-$ nanocomplexes instead

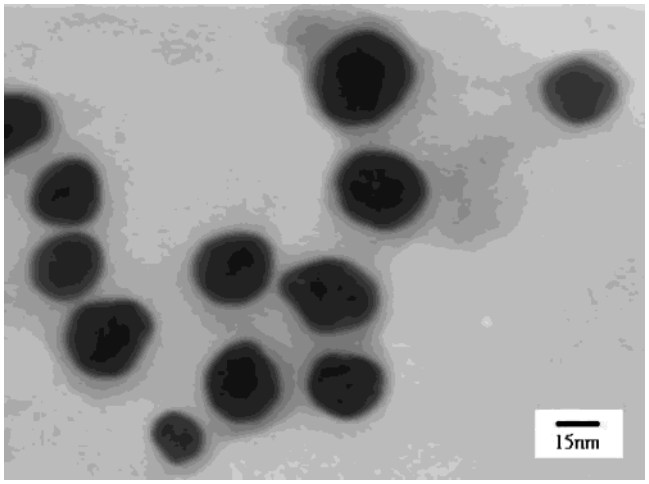

Figure 7. TEM micrograph of Au/PPy core−shell nanocomposites. Preparation conditions: 0.1 mmol/L pyrrole monomer was added into the Au-containing nanocomplexes in solution after roughening Au substrate with 100 scans.

of on an individual $AuCl_4^-$ nanocomplex. The core−shell structure has a diameter of ca. 30 nm. Because the elemental Au is completely coated with a shell of PPy, no characteristic absorption band of elemental Au(0) nanoparticles is shown in the UV−vis spectrum. The existence of the Au(0) core can be confirmed by the XPS spectrum. The XPS measuring depth is much deeper than that of the UV−vis absorption analysis. In the system of PPy electrodeposited on a Au substrate, our experience tells us that more than a 20-nm thickness of the PPy deposition is necessary to shield the signal of the Au substrate shown in the XPS spectrum. As shown in Figure 7, the thickness of the PPy shell is only about 5 nm. As a result, the signal of the elemental Au after PPy growth is shown in the XPS spectrum (data not shown here).

Conclusion

In summary, we have developed an easy electrochemical way to prepare Au-containing nanocomplexes with controllable particle sizes. The prepared nanocomplex size increases from 2 to 50 nm with the increase of the ORC scan from 25 to 400 cycles. On the basis of these nanocomplexes, Au/PPy nanocomposites with a core−shell structure are prepared. Also, elemental Au nanoparticles can possibly be prepared by electrosonification methods. The study on the potential application of this methodology to other noble metals or bimetals is currently underway.

Acknowledgment. The authors thank the National Science Council of the Republic of China (NSC-91-2214-E-238-001) and Vanung University for their financial support. Help from undergraduate student Cheng-Jung Tsai is acknowledged.

References and Notes

(1) Templeton, A. C.; Pietron, J. J.; Murray, R. W.; Mulvaney, P. *J. Phys. Chem. B* **2000**, *104*, 564.

(2) Demaille, C.; Brust, M.; Tsionsky, M.; Bard, A. J. *Anal. Chem.* **1997**, *69*, 2323.

(3) Chandrasekharan, N.; Kamat, P. V. *J. Phys. Chem. B* **2000**, *104*, 10851.

(4) Peto, G.; Molnar, G. L.; Paszti, Z.; Geszti, O.; Beck, A.; Guczi, L. *Mater. Sci. Eng., C* **2002**, *19*, 95.

(5) *Clusters and Colloids*; Schmid, G., Ed.; VCH: Weinheim, Germany, 1994; p 5.

(6) Pastoriza-Santos, I.; Liz-Marzan, L. M. *Langmuir* **2002**, *18*, 2888.

(7) Mizukoshi, Y.; Okitsu, K.; Maeda, Y.; Yamamoto, T. A.; Oshima, R.; Nagata, Y. *J. Phys. Chem. B* **1997**, *101*, 7033.
(8) Grunes, J.; Zhu, J.; Anderson, E. A.; Somorjai, G. A. *J. Phys. Chem. B* **2002**, *106*, 11463.
(9) Dolgaev, S. I.; Simakin, A. V.; Voronov, V. V.; Shafeev, G. A.; Verduraz, F. B. *Appl. Surf. Sci*. **2002**, *186*, 546.
(10) Henglein, A.; Meisel, D. *Langmuir* **1998**, *14*, 7392.
(11) Bourg, M. C.; Badia, A.; Lennox, R. B. *J. Phys. Chem. B* **2000**, *104*, 6562.
(12) Dawson, A.; Kamat, P. V. *J. Phys. Chem. B* **2001**, *105*, 960.
(13) Link, S.; El-Sayed, M. A. *J. Phys. Chem. B* **1999**, *103*, 8410.
(14) Mafune, F.; Kohno, J. Y.; Takeda, Y.; Kondow, T. *J. Phys. Chem. B* **2001**, *105*, 5114.
(15) Haynes, C. L.; Van Duyne, R. P. *J. Phys. Chem. B* **2001**, *105*, 5599.
(16) Kobayashi, Y.; Correa-Duarte, M. A.; Liz-Marzan, L. M. *Langmuir* **2001**, *17*, 6375.
(17) Wang, T. C.; Rubner, M. F.; Cohen, R. E. *Langmuir* **2002**, *18*, 3370.
(18) Kawakami, Y.; Seto, T.; Yoshida, T.; Ozawa, E. *Appl. Surf. Sci*. **2002**, *197*−*198*, 587.
(19) Esumi, K.; Hosoya, T.; Suzuki, A.; Torigoe, K. *Langmuir* **2000**, *16*, 2978.
(20) Sarathy, K. V.; Raina, G.; Yadav, R. T.; Kulkarni, G. U.; Rao, C. N. R. *J. Phys. Chem. B* **1997**, *101*, 9876.
(21) Zamborini, F. P.; Gross, S. M.; Murray, R. W. *Langmuir* **2001**, *17*, 481.
(22) Antonietti, M.; Forster, S.; Hartmann, S.; Oestreich, S. *Macromolecules* **1996**, *29*, 3800.
(23) Mukerjee, S.; Srinivasan, S. *J. Electroanal. Chem*. **1993**, *357*, 201.
(24) Shin, H. J.; Hwang, I. W.; Hwang, Y. N.; Kim, D.; Han, S. H.; Lee, J. S.; Cho, G. *J. Phys. Chem. B* **2003**, *107*, 4699.
(25) Liu, Y. C.; Yang, K. H.; Wang, C. C. *J. Electroanal. Chem.* **2003**, *549*, 151.
(26) Liu, Y. C.; Hwang, B. J.; Jian, W. J. *Mater. Chem. Phys.* **2002**, *73*, 129.
(27) Liu, Y. C.; Jang, L. Y. *J. Phys. Chem. B* **2002**, *106*, 6748.
(28) Gaur, J. N.; Schmid, G. M. *J. Electroanal. Chem.* **1970**, *24*, 279.
(29) Shipway, A. N.; Lahav, M.; Gabai, R.; Willner, I. *Langmuir* **2000**, *16*, 8789.
(30) Henry, M. C.; Hsueh, C. C.; Timko, B. P.; Freund, M. S. *J. Electrochem. Soc.* **2001**, *148*, D155.
(31) Suzer, S.; Ertas, N.; Kumser, S.; Ataman, O. Y. *Appl. Spectrosc.* **1997**, *51*, 1537.
(32) Gao, P.; Gosztola, D.; Leung, L. W. H.; Weaver, M. J. *J. Electroanal. Chem.* **1987**, *233*, 211.
(33) Liu, Y. C. *Langmuir* **2002**, *18*, 174.
(34) Street, G. B.; Clarke, T. C.; Krounbi, M.; Kanazawa, K.; Lee, V.; Pfluger, P.; Scott, J. C.; Weiser, G. *Mol. Cryst. Liq. Cryst*. **1982**, *83*, 253.